Journal of Turbulence
Volume 7, No. 20, 2006

Taylor & Francis
Taylor & Francis Group

High-resolution direct numerical simulation of turbulence

Y. KANEDA* and T. ISHIHARA

Department of Computational Science and Engineering, Graduate School of Engineering, Nagoya University, Nagoya, 464-8603, Japan

We performed high-resolution direct numerical simulations (DNS) of incompressible turbulence in a periodic box by using a Fourier spectral method with the number of grid points up to 4096^3. The simulations consist of two series: one with $k_{\max}\eta \sim 1$ (series 1), and the other with $k_{\max}\eta \sim 2$ (series 2), where $k_{\max}$ is the highest wavenumber in each simulation, and η is the Kolmogorov length scale. In the 4096^3 DNS, the Taylor scale Reynolds number $R_\lambda \sim 1200$ and the ratio of L/η of the integral length scale L to η is approximately 2200, in series 1. The DNS data analysis reveals simple scaling of various spectra, and also sheds some light on (i) the energy spectrum at high R_λ, (ii) the asymptotic R_λ-dependence of the normalized energy dissipation rate, (iii) the anomalous scaling of the spectra of energy dissipation and enstrophy, and so on. After some preliminary remarks on the methods and limitations of the DNS, this paper presents a review of the DNS data analysis. Discussions are also made on some questions invoked by the DNS.

1. Introduction

One of the main interests in modern turbulence research lies in the exploration of the universal features, or universality, of small-scale statistics in fully developed turbulence. The methods of computational science, especially that of direct numerical simulation (DNS), allow us to solve problems that could not be solved with conventional theoretical methods, and to obtain accurate and detailed information that cannot be obtained experimentally. Their potential importance for the exploration of the universality has been well recognized. Extensive studies have been made for the exploration by such methods, especially by DNS of incompressible turbulence under simple boundary conditions, including the pioneering study by Orszag in 1969 [1]; see, for example [2]–[9].

However, the universality, if it exists, can be expected only at high enough Reynolds number *Re*, and the number of degrees of freedom (DOF) involved in turbulence dynamics increases rapidly with *Re*. It is therefore necessary for the exploration by DNS to deal with a huge number of DOF, while the number of DOF that can be treated is obviously limited by available computer resources.

Fortunately, owing to the recent rapid developments in computational capability, the number of DOF that can be treated in DNS is increasing rapidly. For example, in DNS of incompressible homogeneous turbulence, the number of DOF has increased by a factor of 512 over the past five years or so. The Reynolds numbers achieved in recent DNS are similar to, or sometimes even larger than, those obtained in large laboratory experiments. Such a dramatic quantitative progress is expected to bring about qualitative changes in our understanding of turbulence.

*Corresponding author. E-mail: kaneda@cse.nagoya-u.ac.jp

Journal of Turbulence
ISSN: 1468-5248 (online only)
http://www.tandf.co.uk/journals
DOI: 10.1080/14685240500256099

We recently performed DNS of homogeneous incompressible turbulence by a spectral method with the number of grid points up to 1024^3 on the VPP5000 system at the Information Technology Center of Nagoya University, and DNS up to 4096^3 points on the Earth simulator (ES). The number of DOF in the 4096^3 DNS is $4096^3 \times 4 > 2 \times 10^{11}$, where $4 = 3 + 1$ is the number of DOF (three velocity components and pressure) on each grid point. After preliminary remarks on the method of DNS, this paper presents a review on some of the results of the DNS data analysis. Readers interested in the aspect of parallel computation may refer to [10, 11], the latter of which also presents a brief review on the DNS data analysis.

2. DNS method

The Navier–Stokes (NS) equations for incompressible fluid are just expressions of Newton's law of motion applied to incompressible fluid. They cannot be simplified further without dropping any of the three key ingredients of fluid motion: (i) nonlinear convective effect associated with fluid motion, (ii) dissipation owing to viscosity, and (iii) mass conservation, or the incompressibility condition. In this sense, the system of the NS equations may be regarded as the simplest among those keeping the essence of turbulence dynamics.

We simulated the motion of an incompressible fluid by solving the NS equations with periodic boundary conditions (BC). The use of simple BC such as the periodic BC in the study of small-scale statistics is supported by the widely accepted idea that the statistics is insensitive to the details of large-scale conditions, at sufficiently high *Re*.

Our simulations use a fourth-order Runge–Kutta method for time advancing and a Fourier spectral method. Spectral methods have an advantage over conventional finite difference schemes because they enable us to solve accurately and efficiently the Poisson equation for pressure, which results from the mass conservation law. This advantage is attractive especially for DNS of turbulence at high *Re*, where high computational accuracy is required to resolve the motions of small eddies, the velocity amplitudes of which are much smaller than those of large eddies. In our DNS, aliasing errors are removed by the so-called phase-shift method, by which we can keep all the Fourier modes satisfying $k < \sqrt{2}N/3$, where k is the wavenumber, N the number of grid points in each of the Cartesian coordinates in real space and both the minimum wavenumber $k_{\min}$ and the wavenumber increment Δk are unity.

One of the most characteristic features of turbulence at high *Re* is the existence of a wide separation between the characteristic length scale L where most of the energy resides and the scale l where it must be dissipated by viscosity. For the study of high *Re* turbulence by DNS, it is desirable to simulate turbulence with separation between L and l as wide as possible.

In order to obtain some idea of the number of grid points required in DNS, let us divide the total wavenumber range $[k_{\min}, k_{\max}]$ into three ranges as in figure 1: low wavenumber range (L), $k_{\min} \le k < K_L$; medium wavenumber range (M), $k_L \le k < k_l$; and high wavenumber range (H), $k_l \le k \le k_{\max}$, where $k_L = \pi/L$, k_l is the wavenumber at the peak of the energy dissipation spectrum, and $k_{\max}/\Delta k = cN$ with c being a constant of order unity depending on the numerical scheme. In our DNS, $c = \sqrt{2}/3$.

We then have the following estimate

$$cN = \frac{k_{\max}}{\Delta k} = \frac{k_l}{k_{\min}} \times \frac{k_L}{k_L} \times \frac{k_{\max}}{k_l} = c \times \frac{L_{\text{box}}}{L} \times \frac{L}{l} \times \frac{l}{\Delta x} \tag{1}$$

where $\Delta k = k_{\min}$, $L_{\text{box}} = 2\pi/\Delta k$ is the size of the periodic box, $l = \pi/k_l$, and $\Delta x = L_{\text{box}}/N$. Since the number N is limited by available computer memory, speed and so on, equation (1) implies that if we wish to increase the width of the range (M): $k_L \le k < k_l$, we are obliged to sacrifice the width of the ranges (H) and/or (L).

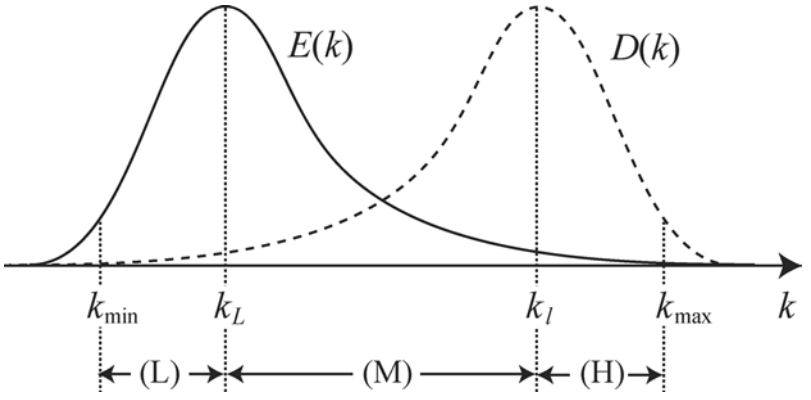

Figure 1. Sketch of wavenumber ranges in DNS of turbulence. $E(k)$ and $D(k) = k^2 E(k)$ are the energy and energy dissipation spectra, respectively, in arbitrary units. (L), (M) and (H) stand for low, medium and high wavenumber ranges, respectively.

Concerning the upper limit wavenumber $k_{\max}$ of the range (H), it is argued that for reliable DNS of small-scale statistics, it desirable to put at least $k_{\max}\eta > 1$ or so, where η is the Kolmogorov length scale defined as $\eta = (\nu^3/\langle\epsilon\rangle)^{1/4}$, and $\langle\epsilon\rangle$ and ν are the mean energy dissipation rate per unit mass and the kinematic viscosity, respectively [6, 12].

Concerning the lower limit wavenumber $k_l = \pi/l$ of the range (H), it has been suggested from DNS, that $k_l\eta$ is then approximately 0.17 (see, for example [13]). The conditions $k_{\max}\eta > 1$ and $k_l\eta = 0.17$ imply $k_{\max}/k_l > 5.9$ or so. If we define Re as $Re = UL/\nu$ and use $\langle\epsilon\rangle \simeq DU^3/L$, then $L/\eta \simeq D^{1/4}Re^{3/4}$, where U is the characteristic velocity of the energy containing eddies, and D is a constant. Consider, for example, DNS with $N = 1024$, $c = \sqrt{2}/3$, and $k_{\max}/k_l > 5.9$. Then equation (1) gives the inequality

$$82 > \frac{k_L}{k_{\min}} \times \frac{k_l}{k_L} \simeq \frac{k_L}{k_{\min}} \times (0.043 \times Re^{3/4})$$

where we have put $D \sim 0.4$ (see figure 5 in section 4) and used $k_l\eta = 0.17$. Thus, even in DNS with Nas large as $N = 1024$ and k_L as small as $k_L/k_{\min} = 3$, we have the limitation that $k_L/k_l < 27$ and $Re < 5.5 \times 10^3$.

Regarding the possible influence of the wavenumber truncation at $k = k_{\max}$, a comparison of DNS with different resolution $k_{\max}\eta \simeq 0.5$, 1.0 and 2.0 shows that the solution trajectories in the phase space are in fact sensitive to the resolution level, as would be expected. However, it also suggests that low-order statistics such as the energy and energy dissipation spectra are insensitive to the difference, especially at low k, under certain conditions [12].

As for the width of the range (L), where $k_{\min} < k < k_L$, it is generally thought that the small-scale statistics in (H) is not sensitive to the width nor to the detail of the conditions such as forcing in (L). The width can, however, significantly affect large-scale statistics, such as the Loitsyansky's integral and the final period of decay (see, for example, [14, 15]).

Another concern in performing DNS at high Re may be the possible influence of arithmetic precision. The amplitudes of smallest eddies can be very small as compared with those of energy-containing eddies in turbulence at high Re, so that for resolving the motions of the small eddies high accuracy or arithmetic precision are needed. We have made some comparisons between DNS with single- and double-precision arithmetic with $N = 1024$. The effect of reducing the precision was seen to be insignificant, at least for low-order statistics such as the energy spectrum [10, 16].

3. DNS on VPP5000

The VPP5000 system at the Information Technology Center of Nagoya University has approximately 1.0 TB total main memory and theoretical peak performance of 0.6 Tflops. By using the system, we have performed DNS of incompressible turbulence obeying the NS equations with and without the mean flow of a simple shearing motion. The Taylor scale Reynolds numbers R_λ about 470 (280) was achieved by the DNS with $k_{\max}\eta \simeq 1 (k_{\max}\eta \simeq 2)$ and 1024^3 grid points.

The DNS provide us with valuable data for the study of turbulence dynamics free from experimental uncertainties. The DNS data have been used for analysing turbulence statistics, including the following scaling. The study of scaling in turbulence is of interest not only from the theoretical point of view, but also from the practical point of view especially because the understanding may give some idea on how to modify the parameters in turbulence modelling when the grid size is changed.

3.1 *Energy spectrum*

The energy spectrum $E(k) = (1/2)\sum_{p=k} Q_{ii}(\mathbf{p})$ in the inertial subrange (ISR) fits fairly well to the $k^{-5/3}$ law, where $Q_{ij}(\mathbf{p}) \equiv Q_{ij}(\mathbf{p}, t, t)$, $Q_{ij}(\mathbf{p}, t', t) = \langle \hat{v}_i(\mathbf{p}, t')\hat{v}_j(-\mathbf{p}, t)\rangle$, the summation convention is used for the repeated indices, $\hat{v}_i(\mathbf{p})$ the Fourier transform of the ith velocity component v_i with respect to the position vector $\mathbf{x}$, $\langle\rangle$ the ensemble average, $\mathbf{p}$ the wave vector, and $\sum_{p=k}$ denotes the integral or the summation with respect to $\mathbf{p}$ over a spherical shell that satisfies $k - 1/2 < p \leq k + 1/2$ [8].

3.2 *Microtime scales*

The Eulerian and Lagrangian microtime scales $\tau_E(k)$ and $\tau_L(k)$ scale as $\tau_E(k) \propto k^{-1}$ and $\tau_L(k) \propto k^{-2/3}$ in the ISR, where

$$\tau_X(k)^2 \equiv -\frac{\partial^2 Q_X(k, t+\tau, t)/\partial\tau^2|_{\tau=0}}{Q_X(k, t, t)}$$

$X = E$ or L, $Q_X(k, t', t) = (1/2)\sum_{k'=k} Q_X(\mathbf{k}', t', t)$, $Q_E(\mathbf{k}, t', t) = Q_{ii}(\mathbf{k}, t', t)$, $Q_L(\mathbf{k}, t, t') = \langle \hat{v}_i; (\mathbf{k}, t|t')\hat{v}_i(-\mathbf{k}, t)\rangle$, and $\hat{v}_i(\mathbf{k}, t'|t)$ is the Fourier transform of the velocity $\hat{v}_i(\mathbf{x}, t'|t)$ with respect to $\mathbf{x}$ at time t of the fluid particle that was at position $\mathbf{x}$ at time t [17]. The scaling $\tau_E(k) \propto k^{-1}$ supports the idea of the dominance of the random sweeping effect by large eddies.

3.3 *Anisotropy in homogeneous turbulent shear flow*

In DNS of homogeneous turbulent shear flow under periodic BC with the mean flow of a simple shearing motion, $Q_{ij}(\mathbf{k})$ is almost, but not exactly, isotropic, at small scales, while the spectra of the anisotropic components, such as $E_{\alpha\beta}(k)$, $E_{ii}^{\alpha\beta}(k)$ and $E_{\alpha\beta}^{ii}(k)$, $(\alpha \neq \beta)$ fit well to the scaling k^{-m} with $m \simeq 7/3$ in the ISR, provided that they are not zero, where

$$E_{\alpha\beta}(k) \equiv \sum_{p=k} Q_{\alpha\beta}(\mathbf{p}), \quad E_{ij}^{\alpha\beta}(k) \equiv \sum_{p=k} p_\alpha p_\beta Q_{ij}(\mathbf{p})/p^2$$

These spectra must be zero in isotropic turbulence for $\alpha \neq \beta$ [18, 19].

3.4 *Error growth*

A comparison between DNS with different resolution noted in section 2 suggests that the error attributed to wavenumber truncation at $k = k_{\max}$ increases faster at higher k, and the error spectrum obeys a simple scaling in k in the ISR, $k \ll k_{\max}$. The growth is algebraic, not exponential, in time [12].

3.5 *Turbulent diffusion*

Lagrangian one- and two-point statistics were analysed by tracking n-fluid particles, with n being order 10^5, in isotropic turbulence generated by the DNS with 1024^3 grid points, where a cubic spline interpolation method was used to compute the fluid particle velocity as in [20]. The mean square of the difference $\delta\mathbf{v} = \mathbf{v}(t+\tau) - \mathbf{v}(t)$ between time interval τ of the Lagrangian velocity $\mathbf{v}$ of a fluid particle moving with the fluid scales such as $\langle|\delta\mathbf{v}|^2\rangle \propto \tau$ in the ISR. The mean square of the distance vector between two fluid particles, which were initially close to each other, grows with time t as $\propto t^3$ in the ISR. A simple spectral closure approximation is shown to be in good agreement with the DNS [21].

4. DNS on the Earth simulator (ES)

The ES has approximately 10 TB total main memory and 40 Tflops theoretical peak performance. Sustained performance of 16.4 Tflops was achieved for the 2048^3 DNS using a spectral method on the ES [10].

We performed two series of DNS of forced turbulence up to $N = 4096$: one with $k_{\max}\eta \sim 1$ (series 1), and the other with $k_{\max}\eta \sim 2$ (series 2). Forcing was achieved by introducing a negative viscosity coefficient for all the Fourier modes with wavenumbers $k = |\mathbf{k}| < 2.5$, i.e. we added a term $\hat{\mathbf{F}}(\mathbf{k}) = c\hat{\mathbf{u}}(\mathbf{k})$ to the NS-equations in the wave vector space, where $\hat{\mathbf{u}}(\mathbf{k})$ is the Fourier transform of the velocity vector $\mathbf{u}(\mathbf{x})$ and $c = 0$ for $k \geq 2.5$. The magnitude of the constant c is adjusted at each time step to keep the total kinetic energy E constant [12]. We chose to force the field in a deterministic way, because we are interested in the intrinsic randomness owing to the turbulence dynamics, and wish to avoid mixing the randomness with that in the forcing; see for example, the discussion in [4]. We confined the forcing only to a low wavenumber range, because we are interested in the possible universality at small scales. Underlying our use of such forcing is Kolmogorov's idea, according to which the small-scale statistics is insensitive to the details of the forcing or boundary conditions at large scales.

Double-precision arithmetics were used in the DNS, except the 4096^3 DNS for which, in order to save the required machine memory, we reduced partly the precision of arithmetic from double to single, but used double-precision arithmetics for computing the nonlinear convolution sums. The effect of reducing the precision was confirmed to be insignificant, at least for low-order statistics such as the energy spectrum, in preliminary DNS with $N = 1024$.

Some representative values characterizing the runs are shown in figure 2, where the values were measured at almost stationary states. Figure 2(a) shows $Re = u'L/\nu$ and the Taylor scale Reynolds number R_λ versus N, while figure 2(b) shows L/η and λ/η versus Re, where $\eta = (\nu^3/\langle\epsilon\rangle)^{1/4}$, and L and λ are respectively the integral length scale defined by

$$L \equiv \frac{\pi}{2u'^2}\int_0^{k_{\max}} E(k)/k\,dk$$

and the Taylor microscale $\lambda = (15\nu u'^2/\langle\epsilon\rangle)^{1/2}$, with $3u'^2/2 = E$. These figures are made from the data in [8, 13]. In the 4096^3 DNS, $R_\lambda \sim 1200$ and $L/\eta \sim 2200$ in series 1, and $R_\lambda \sim 675$

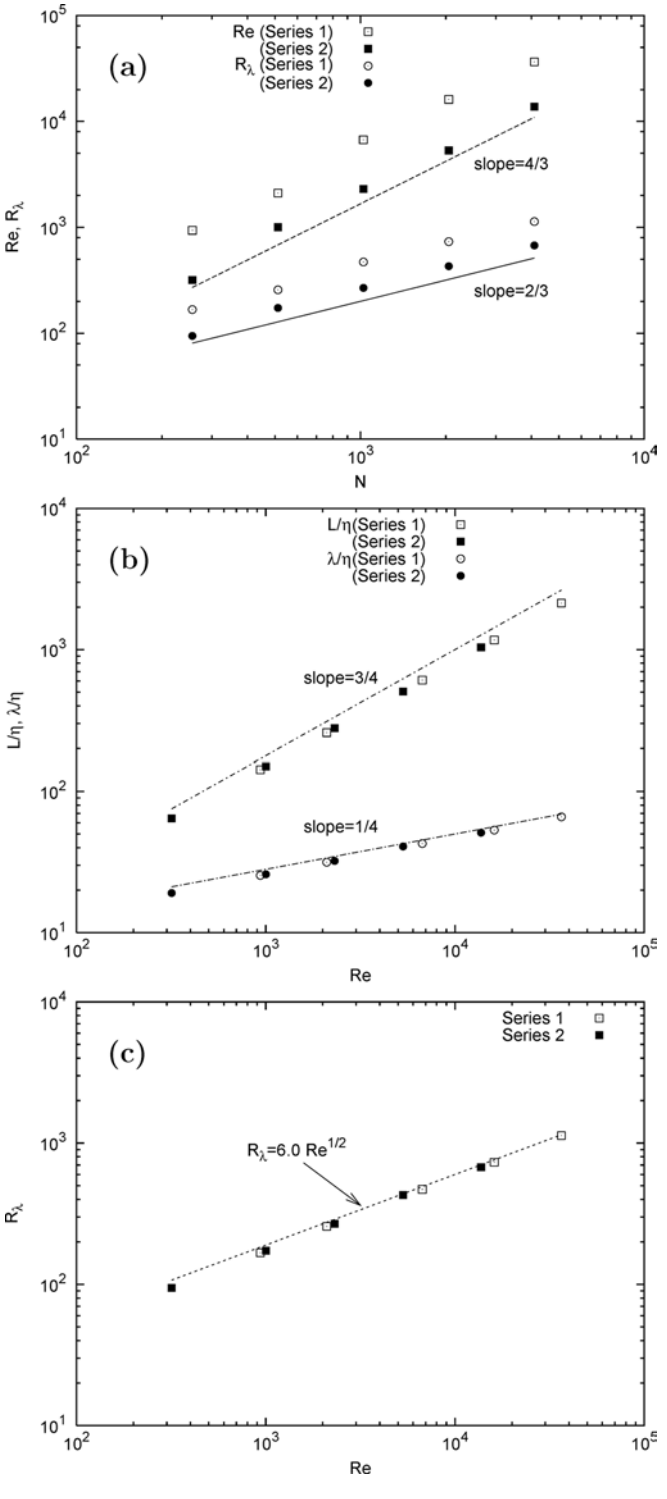

Figure 2. (a) Re and R_λ versus N; (b) L/η and λ/η versus Re; and (c) R_λ versus Re.

and $L/\eta \sim 1040$ in series 2. The ratio $L/\eta \sim 2200$ in the 4096^3 DNS of series 1, is much larger than, for example, $L/\eta \sim 140$ in the 256^3 DNS of series 1.

The figures provide a confirmation of the well-known scaling

$$N \propto Re^{3/4}, \quad N \propto R_\lambda^{3/2}$$

and

$$L/\eta \alpha Re^{3/4}, \quad \lambda/\eta \propto Re^{1/4}$$

which are derived by a simple dimensional analysis using Kolmogorov's scaling. Similarly figure 2(c) gives a confirmation of the scaling

$$R_\lambda \propto Re^{1/2}$$

A line in the figure denotes $R_\lambda = C\ Re^{1/2}$ with $C = 6.0$, the value of which is obtained by $C = (15/D)^{1/2}$ with $D \approx 0.4$ (see section 4.3).

4.1 *Visualization of intense vorticity region*

Before discussing quantitative aspects of the DNS data analysis, it may be interesting to have some intuitive idea on the field which we are considering, through the help of visualization. Figure 3 shows the intense vorticity field where the vorticity $\omega > \langle\omega\rangle + 4\sigma_\omega$ from the 2048^3 DNS data. Here $\omega = |\boldsymbol{\omega}|$, $\langle\omega\rangle$ is the spatial average of ω and σ_ω the standard deviation of ω. Figures 3(b), (c) and (d) show the close-up view of the central region of figures 3(a), (b) and (c), respectively. Figure 3 is compiled from figures 4–7 in [10] by adding the characteristic scales L, λ and η. As seen from the comparison of the scales L, λ and η shown on the figures, the vorticity distribution in a wide range of scales is shown. Figure 4 shows the intense vorticity region by a lower-resolution DNS with $N = 256$. At low or moderate Reynolds number DNS, such as DNS with $N \leq 256$ or so, the visualization might give an impression that the whole flow field is dominated by a few numbers of intense vortices, but figure 3 shows that this is not the case.

4.2 *Energy flux*

The data of high-resolution DNS present features of turbulence dynamics that have not been captured by previous lower-resolution DNS. An example of such features is seen in the data for the energy flux $\Pi(k)$ across the wavenumber k. In theories of turbulence, it is often assumed that in the wavenumber range of k such that $k_L \ll k \ll k_l$, $\Pi(k)$ is constant independent of k and $\Pi(k) = \langle\epsilon\rangle$ in a statistically steady state of turbulence. However, in DNS with $N \leq 1024$ or so, the range satisfying such independence is quite narrow, and $\Pi(k) \simeq \langle\epsilon\rangle$ is not well satisfied [8]. In contrast, the range in 2048^3 and 4096^3 DNS is much wider than that in these DNS, and $\Pi(k) \simeq \langle\epsilon\rangle$ in the range. This implies that the 2048^3 and 4096^3 DNS exhibit the ISR much wider than those in previous DNS, and therefore provide invaluable data for exploring universal nature of turbulence at high Re.

4.3 *Normalized dissipation rate*

Another example of features captured by high-resolution DNS is shown in figure 5, which is from [16]. It shows the normalized dissipation rate $D = \langle\epsilon\rangle L/U^3$ including the data collected in [8, 22]. As noted by Sreenivasan [22], the independence of D from ν for large Re is a

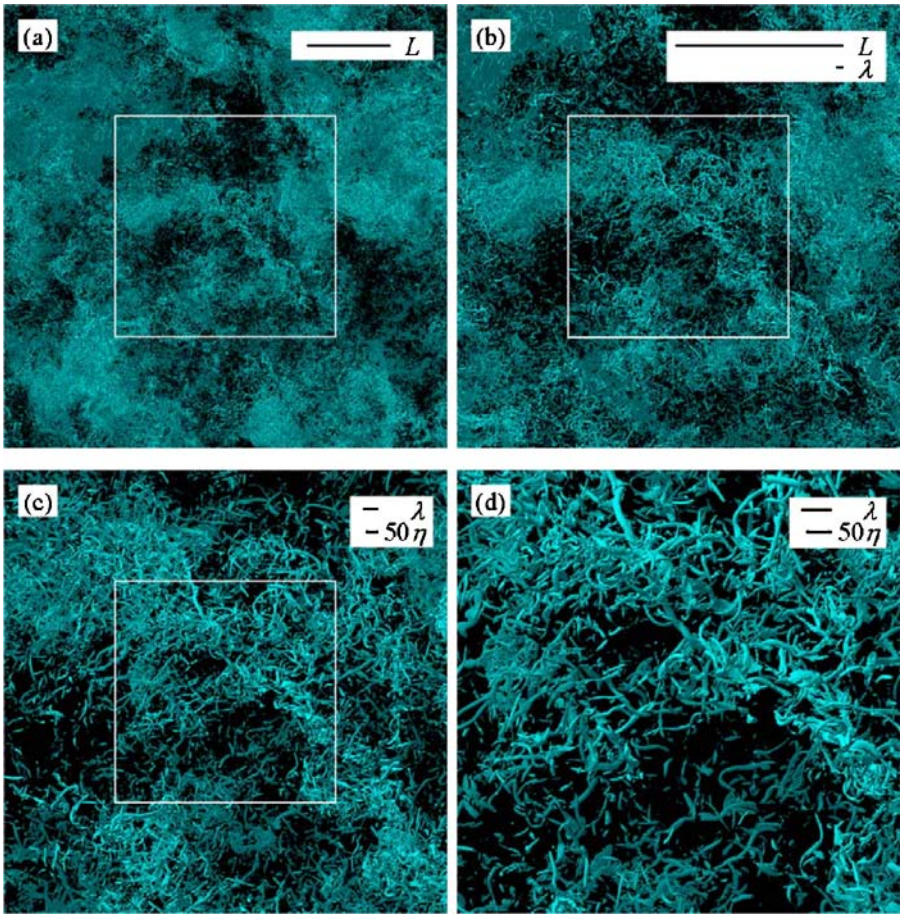

Figure 3. Intense-vorticity isosurfaces showing the region where $\omega > \langle\omega\rangle + 4\sigma_\omega$. $R_\lambda = 732$. (a) The size of the display domain is $(5984^2 \times 1496)\,\eta^3$, periodic in the vertical and horizontal directions. (b) Close-up view of the central region of (a) bounded by the white rectangular line; the size of display domain is $(2992^2 \times 1496)\,\eta^3$. (c) Close-up view of the central region of (b); $1496^3\eta^3$ (d) Close-up view of the central region of (c); $(748^2 \times 1496)\,\eta^3$.

basic premise in the phenomenology of turbulence. The data for $R_\lambda \leq 200$ or so in figure 5 show that D decreases monotonically with R_λ, but it is not very clear whether D would really tend to nonzero constant for large R_λ, if the data $R_\lambda > 200$ were not available. In contrast, the data including $R_\lambda > 200$ or so strongly suggest that D tends to a nonzero constant ($\approx$0.4) as $R_\lambda \to \infty$.

4.4 *Energy spectrum*

Besides the normalized dissipation rate, another quantity of fundamental interest in turbulence theory is the energy spectrum. Figure 6(a) shows the pre-multiplied energy and energy dissipation spectra $kE(k)/E_0$ and $kD(k)/D_0$ versus $k\eta$, where $E_0 = \int E(k)dk$, $D(k) = k^2E(k)$ and $D_0 = \int D(k)dk$. Figure 6(b) shows the plot against kL. In figure 6, it is seen that the curves for $E(k)/E_0$ and $D(k)/D_0$ overlap well when plotted against kL and $k\eta$, respectively.

Figures 6(c) and (d) show the same data but as log-log plots of $E(k)$ versus $k\eta$ and kL, respectively. It might be thought from figures 6(c) and (d) that the DNS spectra fit quite well to Kolmogorov's $k^{-5/3}$ law. However, a close inspection of the compensated energy spectrum

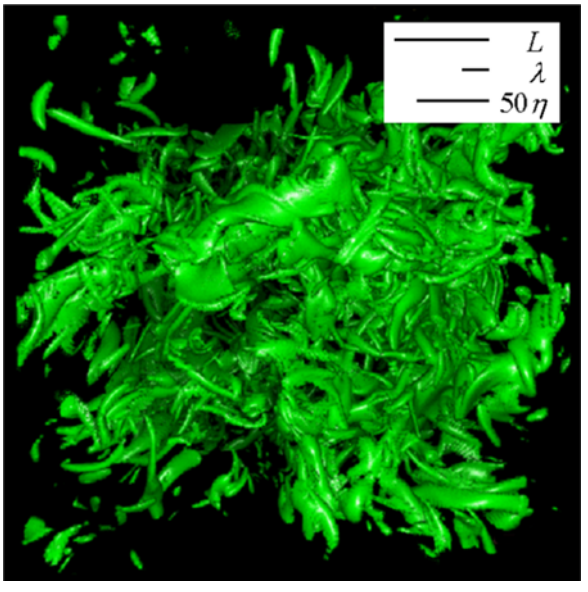

Figure 4. Intense-vorticity isosurfaces showing the region where $\omega > \langle\omega\rangle + 4\sigma_\omega$. The size of the display domain is $367^3\eta^3$, periodic in the vertical and horizontal directions. $R_\lambda = 94$.

$k^{3/5}E(k)$ (see figure 5 in [16]) reveals that the energy spectrum in the 2048^3 and 4096^3 DNS fits in the ISR to $E(k) \propto^{-5/3-\mu}$ where $\mu \simeq 0.1$.

Regarding the correction μ for $Re \to \infty$, there are at least two possibilities: (i) it tends to zero, and (ii) it remains at nonzero owing to, for example, intermittency. At present the possibility that the finiteness of *Re* and that of the width of the ISR play important roles for the correction is not excluded. Here the 'finiteness' of the width means not only the finiteness of the range, but also that there may be contributions from nonlinear interactions between eddies in the ISR and eddies outside the range (small scale and large scale) where the scaling does not apply. It would be interesting to study the effects of the finiteness of *Re* as well as that of the width of the ISR, before settling the issue of the correction (see section 4.6).

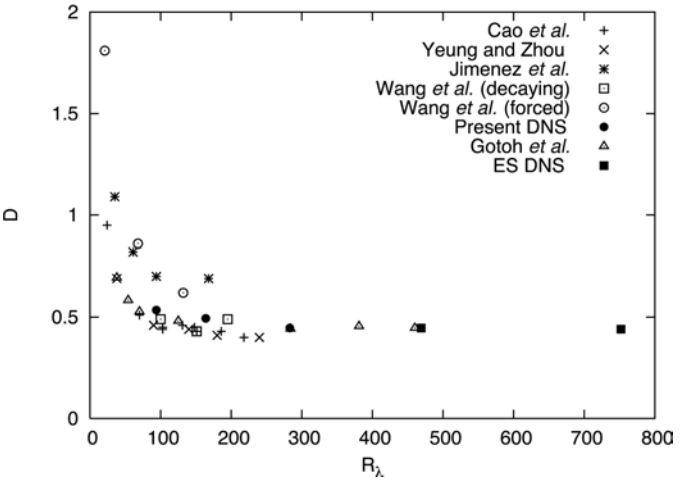

Figure 5. Normalized dissipation rate D versus R_λ. From [16].

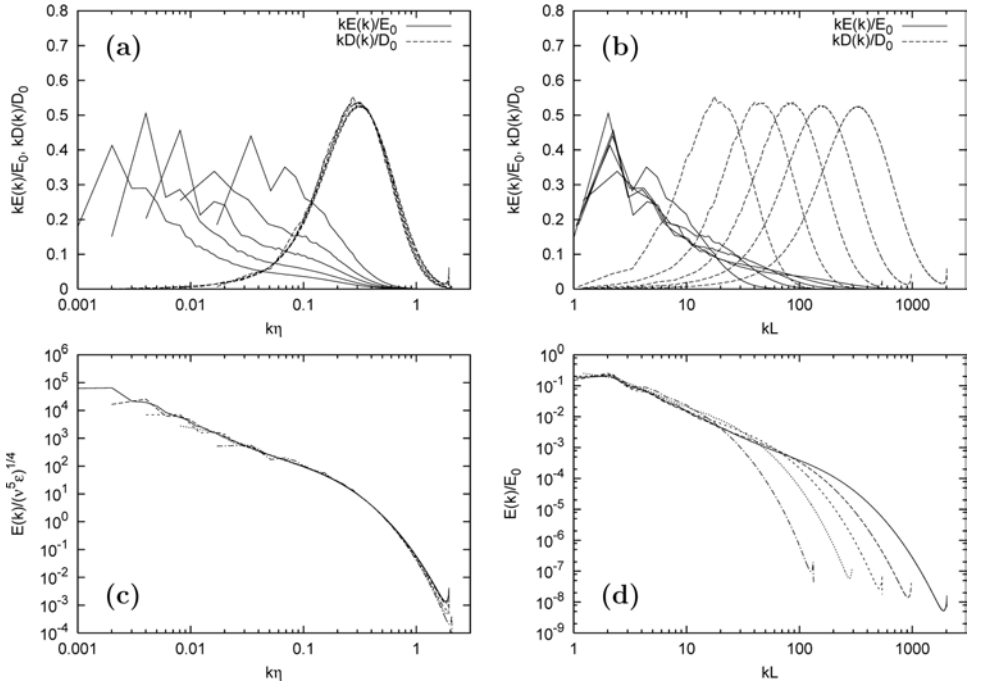

Figure 6. (a) Pre-multiplied energy and dissipation spectra $kE(k)/E_0$ and $kD(k)/D_0$ versus $k\eta$ obtained by the DNS of series 2 with $N = 256$, 512, 1024, 2048 and 4096. (b) The data are the same as for (a) but against kL. (c) $E(k)/\nu^5\,\langle\epsilon\rangle^{1/4}$ versus $k\eta$. (d) $E(k)/E_0$ versus kL.

4.5 *Spectra of energy dissipation, enstrophy and pressure*

The statistics or the intermittency of the rate $\epsilon(= 2\nu s^2)$ of energy dissipation per unit mass plays an important role in turbulence theories, where $s^2 = s_{ij}s_{ij}$ and s_{ij} is the rate-of-strain tensor. The vorticity $\boldsymbol{\omega} = \mathrm{rot}\mathbf{u}$ has also been the subject of intensive studies. Since s, ω and pressure p satisfy the relationship $s^2 - \omega^2/2 = -\Delta p$, it follows that

$$\int_V s^2 dV - \int_V \frac{1}{2}\omega^2 dV = -\int_{\partial V} \mathbf{n}\cdot\nabla p dS \tag{2}$$

for any region V, where $\int_V dV$ is the volume integral over a volume V and $\int_{\partial V} dS$ is the surface integral over the surface ∂V of V. Note that the integrands in the first and second volume integrals on the left-hand side of equation (2) are non-negative, so that the two integrals increase with $V(\equiv L^3)$ roughly in proportion to L^3, whereas the surface integral on the right-hand side of equation (2) increases with L in proportion to at most only L^2. This suggests that for large enough L, the difference between the volume averages of $\omega/2$ and $s^2 = \langle\epsilon\rangle/(2\nu)$ is small.

Figures 7(a) and (b), which are from [23], show three-dimensional snapshots of intense vorticity and dissipation fields, respectively, obtained by DNS with $N = 512$, $R_\lambda = 164$. Figure 7(c) shows the overlap of figures 7(a) and (b). Figures 8(a), (b) and (c) are from the same DNS field, but show the intensity on a plane. Visualizations similar to figure 7(a) have been also obtained by previous DNS studies, for example [3, 4, 24] ([24] is by DNS for slightly compressible turbulence). Visualizations similar to figure 7(c) were shown in [3], in which $R_\lambda = 82.9$. It is seen from figures 7 and 8 that the shape of intense ω regions are tube- or worm-like, whereas those of intense ϵ regions are petal- or fan-like. The locations of intense ϵ are near the intense vortex tube. These observations are consistent with previous reports, such

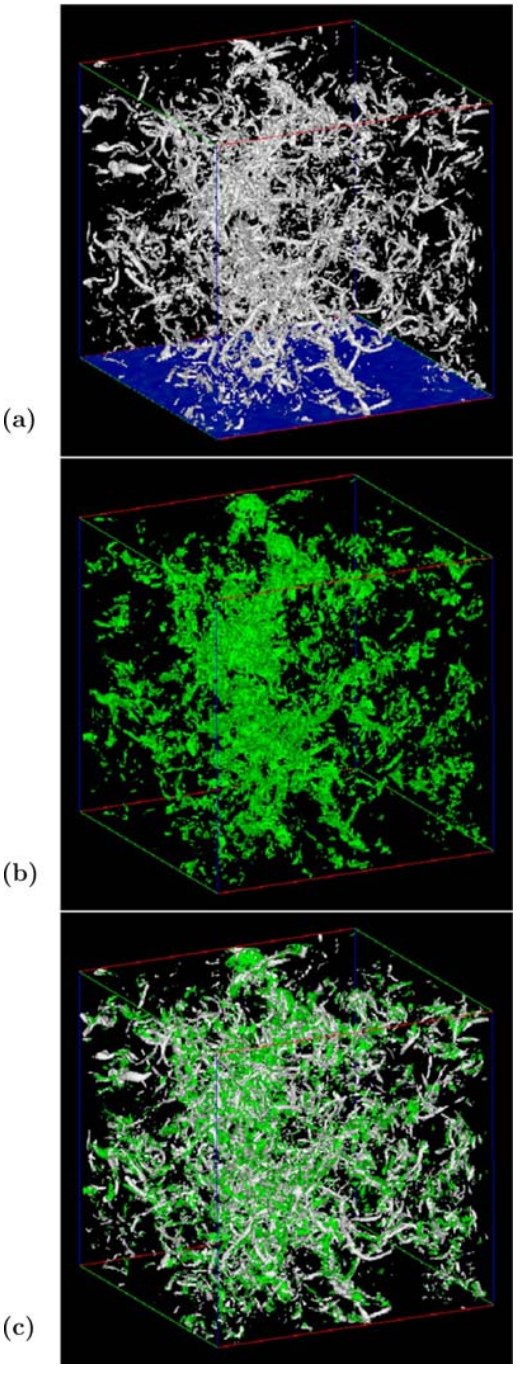

Figure 7. Intense (a) vorticity and (b) dissipation isosurfaces showing the region where $\omega > \langle\omega\rangle + 3\sigma_\omega$ and $\epsilon > \langle\epsilon\rangle + 3\sigma_\omega$, respectively. From [23]. (c) Overlap of (a) and (b). $R_\lambda = 167$.

as [3, 4, 23, 24]. Figure 7 also shows that, while the locations of the intense ω and ϵ regions are close to each other in a coarse-grained scale [23], they are not so close on a closer view.

One of the most basic and simplest measures characterizing the intermittency of these fields is the spectrum $E_f(k) = \sum_k \langle \hat{f}(\mathbf{k})\hat{f}(-\mathbf{k})\rangle$, where $f = \Omega = \omega^2/2$ or ϵ and $\hat{f}(\mathbf{k})$ is the Fourier

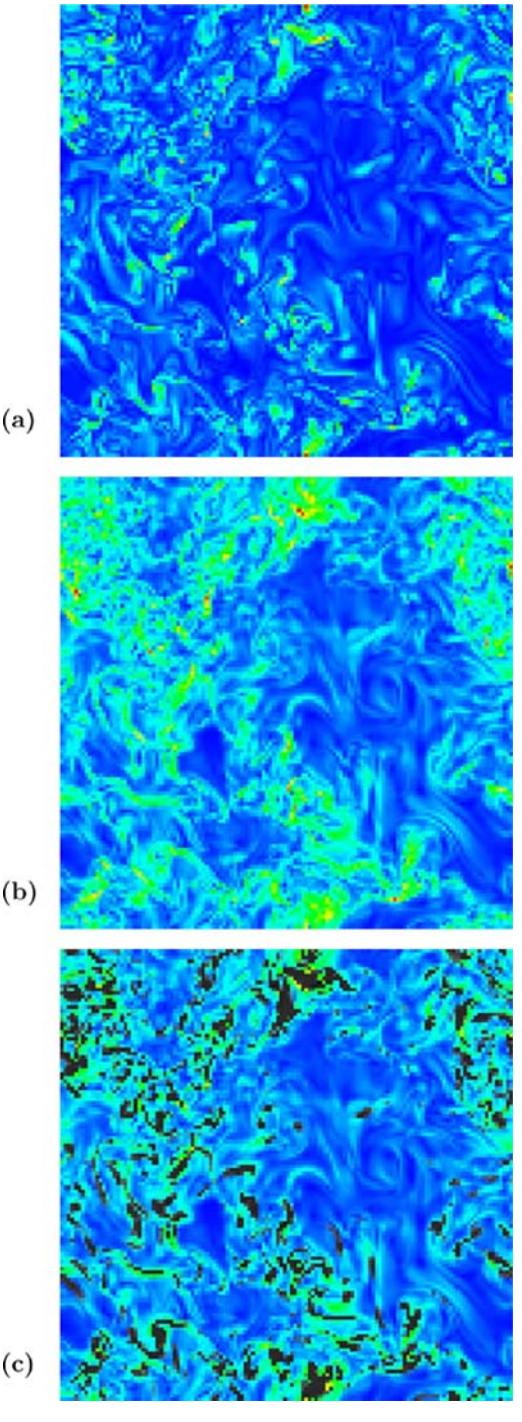

Figure 8. (a) Contour plot of vorticity on a plane of turbulent velocity field and (b) Contour plot of dissipation on the same plane as (a). (c) The same as (b) but the regions where $\omega > \langle\omega\rangle + 3\sigma_\omega$ are shown by black.

transform of f. A simple dimensional argument using $\langle\epsilon\rangle$ and k would give $E_\epsilon(k) \propto k^{5/3}$ and $E_\Omega(k) \propto k^{5/3}$. Similarly, $E_{\nabla^2 p}(k)$ is also shown to scale as $\propto k^{5/3}$ in the ISR, where p is the pressure.

On the other hand, according to the high-resolution DNS, the spectra $E_\epsilon(k)$ and $E_\Omega(k)$ exhibit a range in which they scale with k differently from the Kolmogorov scaling, as shown in previous studies. Our DNS shows that they scale as $\propto k^a$ in the ISR, where the exponent a is approximately $-2/3$ for $E_\epsilon(k)$ and E_Ω, whereas a is approximately 1.81 for $E_{\nabla^2 p}(k)$ in fairly close agreement with the Kolmogorov scaling [25].

The DNS also shows that the difference between the spectra $E_{s^2}(k) = E_\epsilon(k)/(2\nu)^2$ and $E_\Omega(k)$ is small over a certain wave number range at small k, but the difference [with $E_\Omega(k) > E_{s^2}(k)$] is large at higher k, and the difference peaks at $k\eta \approx 0.4$ [25]. These facts are consistent with the observations noted above, i.e. (i) the intense ω and ϵ regions are located close to each other at large scales, but (ii) not only their shapes but also their locations are different from each other at small scales. The similarity of two spectra at low k (large scale) is also consistent with the small difference between the first and second volume integral in the left-hand side of equation (2) for large V. In order to explain the difference between the two spectra at high k, we have to take into account the fine-scale structures of ϵ and ω. Such an explanation remains to be explored.

4.6 *Reynolds number dependence of statistics*

In studies of turbulence, it is often mentioned that universality in turbulence at sufficiently large Reynolds number can be expected. However, the Reynolds number cannot be infinite in real turbulence, and little seems known about the quantitative aspect of this statement. For example, we may ask if $R_\lambda = 10{,}000$ is large enough for the appearance of the universality under consideration. What is lacking here is the quantitative understanding of the Reynolds number dependence of the statistics.

In this respect, we recently studied the energy spectrum in the near dissipation range (DR). According to the Kolmogorov hypotheses the energy spectrum is universal in the equilibrium range, and experiments and DNS suggest that the effect of intermittency on the energy spectrum is weak. Previous studies suggested that DNS spectra for $R_\lambda < 100$ fit well to the form $E(k) = C\ (k\eta)^\alpha\ \exp\ (-\beta k\eta)$ in the near DR, where C, α and β are constants independent of k. (see [26] and references cited therein). Our analysis suggests that the DNS spectra for $94 \leq R_\lambda \leq 675$ continue to fit well to the form in the near DR ($0.5 \lesssim k\eta \lesssim 1.5$) and that the values of α and β decrease monotonically with R_λ, and approach R_λ-independent constants as $R_\lambda \to \infty$, in accordance with the Kolmogorov hypotheses, but the approach, especially that of β, is very slow. For example, according to a curve-fitting based on the DNS data, $|\beta(R_\lambda) - \beta(R_\lambda = \infty)\ |/\beta(R_\lambda = \infty)$ is still as large as 2.61, even at $R_\lambda = 10,000$ [13].

We have also studied the Reynolds number dependence of the one-point statistics of velocity derivatives as well as two-point velocity statistics. The results will be discussed elsewhere.

5. Questions raised by DNS

The DNS results provoke questions waiting for theoretical challenges. Among them are the following.

5.1 *Small-scale anisotropy. A linear response theory*

According to the Kolmogorov hypotheses, there exists a universal equilibrium range at sufficiently small scale and large *Re*, which is locally homogeneous and isotropic and can be characterized by a few parameters. The results of DNS noted in sections 3.1 and 3.3 are consistent with this idea, in the sense that the anisotropy component is in fact small, especially at high k, as compared with the energy spectrum. The results noted in section 3.3, however, show first that anisotropic components are not very small, and second the existence of simple scaling laws for the anisotropic components in homogeneous turbulent shear flow. How can we derive the anisotropy?

In this regard, it may be interesting to recall that in the statistical mechanics for a thermal equilibrium or nearly equilibrium system, two classes of universal relations characterizing the macroscopic state are known: (i) those characterizing the equilibrium state itself, such as Boyle–Charles' law; and (ii) those characterizing the response to disturbances added to the equilibrium state. This encourages us to explore not only universal relations in turbulence in the sense of (i), but also those in (ii).

A simple analysis based on the NS equations for turbulent shear flow suggests that at sufficiently small scales, the nonlinear interactions between eddies of similar sizes play the dominant roles in determining the equilibrium state, while the interactions of small eddies with the mean shear may be treated as a small disturbance added to the equilibrium state. It is then shown that

$$\Delta Q_{ij}(\mathbf{k}) = C_{ijkm}(\mathbf{k}) S_{ij} \tag{3}$$

for sufficiently high k, where S_{ij} is the local rate of the strain tensor of the mean shear flow, $\Delta Q_{ij}(\mathbf{k}) = \Delta Q_{ij}(\mathbf{k}) - Q^o_{ij}(\mathbf{k})$, Q^o_{ij} the isotropic spectrum in the absence of mean flow, and $C_{ijkm}(\mathbf{k})$ is a fourth-order isotropic tensor depending on $\mathbf{k}$ but independent from S_{ij}, and reflects the equilibrium state. Equation (3) is in good agreement with DNS [18], and can also be derived by a closure theoretical approach. Equation (3) is similar to the stress and rate of strain relationship for Newtonian fluid. Unlike this relationship, however, C_{ijkm} in equation (3) depends on $\mathbf{k}$ and holds only for high k. The reader may refer to [27] for details of the discussion on equation (3) and references, as well as the analysis of small-scale anisotropy in stably stratified turbulence.

5.2 *Anomalous scaling of spectra of fourth-order velocity moments*

Another question raised by the DNS is on the scaling noted in section 4.4. How can we explain the scaling?

All of the spectra $E_\epsilon(k)$, $E_\Omega(k)$ and $E_{\nabla^2 p}(k)$ can be written in the form

$$E_f(\mathbf{k}) = \sum_k \langle f(\mathbf{k}) f(-\mathbf{k}) \rangle, \quad \text{with} \quad f(\mathbf{k}) = C_{abcd} \sum_{\mathbf{k}=\mathbf{r}+\mathbf{q}} r_a q_b \hat{v}_c(\mathbf{r}) \hat{v}_d(\mathbf{q})$$

where $\sum_{\mathbf{k}=\mathbf{r}+\mathbf{q}}$ denotes the sum over $\mathbf{r}$ and $\mathbf{q}$ satisfying $\mathbf{r}+\mathbf{q}=\mathbf{k}$, and C_{abcd} is a fourth-order constant tensor. The difference between the spectra comes only from the difference in C_{abcd}. It is therefore unlikely that any theory discarding the tensorial dependence of C_{abcd} would explain the difference.

It is shown that

$$\langle f(\mathbf{k}) f(-\mathbf{k}) \rangle = \sum_{\mathbf{k}=\mathbf{r}+\mathbf{q}} C_{abcd} \langle r_a q_b \hat{v}_c(\mathbf{r}) \hat{v}_d(\mathbf{q}) f(-\mathbf{k}) \rangle$$

and

$$C_{abcd}\langle r_a q_b \hat{v}_c(\mathbf{r})\hat{v}_d(\mathbf{q}) f(-\mathbf{k})\rangle = r^2 \times O((\mathbf{k}/\mathbf{r})^z), \quad \text{as} \quad \mathbf{k}/\mathbf{r} \to 0,$$

under weak assumptions. Here $z = 2$ for $f = \nabla^2 p$, while $z = 0$ for $f = \Omega$ and $f = \epsilon^2$, because of the incompressibility condition. A preliminary analysis based on a Lagrangian renormalized perturbation approach suggests that the scalings of the spectra are sensitive to this difference.

5.3 *Inertial range structure*

The visualization of the DNS field suggests that the small-scale structures are distinctively different from large-scale structures. For example, figures 3 and 4 show that the structure of each eddy at scales $\sim 10\eta$ is clearly different from that of the cluster of eddies at larger scales $\simeq 100\eta$ or so. They should not be confused.

In practical application such as the large eddy simulation (LES) of turbulence, the understanding of the structure in the ISR is important. A natural question is then how can we quantify the difference of the structure in the ISR from that of the DR, which can be observed in the figures? Research in such a direction has been started [28].

5.4 *Animation*

Turbulence is a phenomenon in space and time, and the field depends not only on the position in space, but also on time. Studies have been made on the time dependence of the statistics, including those on the the Lagrangian and Eulerian micro-time scales as discussed in section 3.2, and the understanding of the time dependence of statistics has played a key role in developing theories, such as Lagrangian spectral closures. However, as compared with the spatial dependence of turbulence statistics, little seems known about the time dependence. The understanding of the time dependence seems interesting not only from theoretical points of view, but also from practical points of view. For example, it might be of interest to explore turbulence models, such as LES models, that incorporate proper understanding on the structure of turbulence not only in space but also in time.

Some intuitive idea on the time dependence of turbulence statistics may be obtained by the help of animation of the turbulence field. Here we present animations made from our DNS on VPP5000 with $N^3 = 512^3$ and $k_{\max}\,\eta \approx 2.1$ (see animation 1). The animations are from $t = 0.0$ to 2.0; the values of $(R_\lambda,\ L/\eta,\ T/\tau_\eta)$ are (164, 147, 22.5) at $t = 0.0$ and (167, 141, 21.5) at $t = 2.0$, where one eddy turnover time T is approximately 2.18 and τ_η is the Kolmogorov time scale. Animation 1(a) shows the motion of intense vorticity field with $\omega > \langle\omega\rangle + 2\sigma_\omega$. while animation 1(b) shows that with $\omega > \langle\omega\rangle + 3\sigma_\omega$.

The following observations are made:

1. The field consists of many tube-like eddies, as well known in previous studies. The eddies seem to keep their identity during the motion.
2. The motion of vortex tubes seems to be advected *passively*; the motions of eddies seem to be a consequence of large-scale motions, rather than the origin of the latter.
3. The lifetime of long tubes is of the order of one eddy turnover time. (Note the motion of a vortex ring going down in the right half, and also a nearly vertical vortex tube that appears and then disappears in the central area.)
4. There are swirling motions of various scales, from large to small, in space as well as in time.

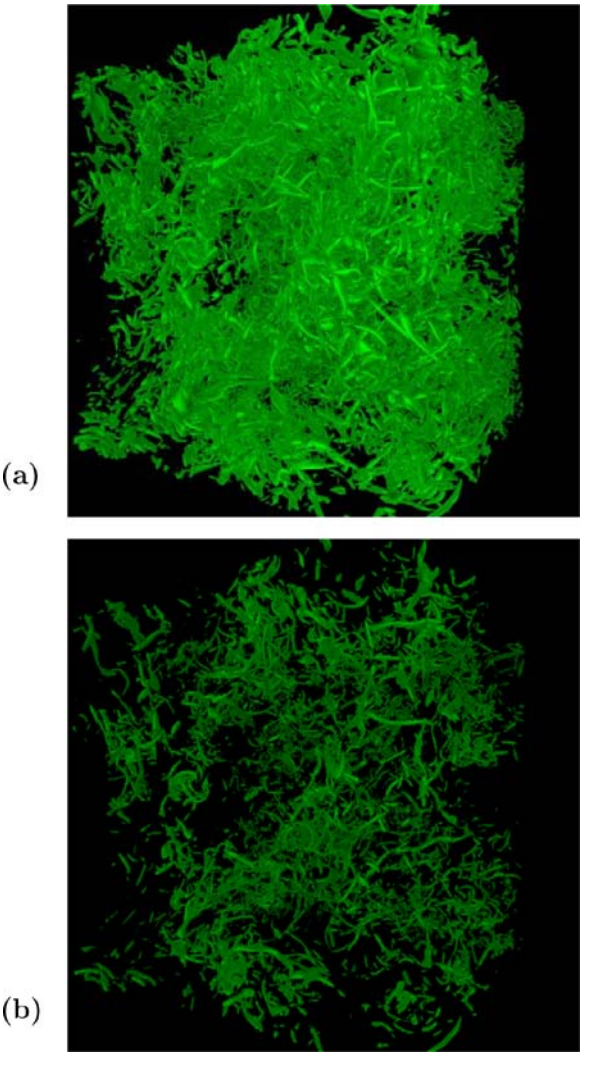

Animation 1. (a) Motion of intense vorticity region with $\omega > \langle\omega\rangle + 2\sigma_\omega$ and (b) that with $\omega > \langle\omega\rangle + 3\sigma_\omega$ from $t = 0.0$ to 2.0.

5. There are regions where the tubes are dense, and where they are sparse. Both of the regions have length scales of approximately L. In the dense regions, the eddies are seen to move actively.
6. In the time scale of one eddy turnover time, the sparse and dense regions continue to be sparse and dense, respectively.

The quantification of such observations remains to be pursued.

Acknowledgements

The DNS studies using the ES and the VPP5000 system were carried out under collaboration with Drs K. Yoshida, M. Yokokawa, K. Itakura and A. Uno. The authors would like to express their thanks to them. They are also grateful to Mr M. Yagyu for his assistance in making the animations. This work was partially supported by Grant-in-Aids for the 21st COE 'Frontiers of

Computational Science', (B)(2)14340033, (B)17340117, (C)(2)15607011, and (C)17560051 from the Japan Society for the Promotion of Science.

References

[1] Orszag, S.A., 1969, Numerical methods for the simulation of turbulence. *Physics of Fluids*, **12**, II-250–257.

[2] Siggia, E.D., 1981, Numerical study of small-scale intermittency in 3-dimensional turbulence. *Journal of Fluid Mechanics*, **107**, 375–406.

[3] Kerr, R.M., 1985, Higher-order derivative correlations and the alignment of small-scale structures in isotropic numerical turbulence. *Journal of Fluid Mechanics*, **153**, 31–58.

[4] Vincent, A. and Meneguzzi, M., 1991, The spatial structure and statistical properties of homogeneous turbulence. *Journal of Fluid Mechanics*, **225**, 1–20.

[5] Chen, S., Doolen, G.D., Kraichnan, R.H. and She, Z.-S., 1993, On statistical correlations between velocity increments and locally averaged dissipation in homogeneous turbulence. *Physics of Fluids A* , **5**, 458–463.

[6] Jimenez, J., Wray, A.A., Saffman, P.G. and Rogallo, R.S., 1993, The structure of intense vorticity in isotropic turbulence. *Journal of Fluid Mechanics*, **225**, 65–90.

[7] Gotoh, T. and Fukayama, D., 2001, Pressure spectrum in homogeneous turbulence. *Physical Review Letters*, **86**, 3775–3778.

[8] Ishihara, T. and Kaneda, Y., 2002, High resolution DNS of incompressible homogeneous forced turbulence - time dependence of the statistics. In: Y. Kaneda and T. Gotoh (Eds) *Statistical Theories and Computational Approaches to Turbulence* (Tokyo: Springer-Verlag), pp. 177–188.

[9] Gotoh, T., Fukayama, D. and Nakano, T., 2002, Velocity field statistics in homogeneous steady turbulence obtained using a high-resolution direct numerical simulation. *Physics of Fluids*, **14**, 1065–1081.

[10] Yokokawa, M., Itakura, K., Uno, A., Ishihara, T. and Kaneda, Y., 2002, 16.4-Tflops direct numerical simulation of turbulence by a Fourier spectral method on the Earth Simulator. *Proceeding of the IEEE/ACM SC2002 Conference* (CD-ROM), Baltimore.

[11] Kaneda, Y. and Yokokawa, M., 2005, DNS of canonical turbulence with up to 4096^3 grid points. In: G. Winter, A. Ecer, J. Periaux, N. Satofuka and P. Fox (Eds), *Parallel Computational Fluid Dynamics 2004* (Amsterdam: Elsevier).

[12] Yamazaki, Y., Ishihara, T. and Kaneda, Y., 2002, Effects of wavenumber truncation on high-resolution direct numerical simulation of turbulence. *Journal of Physics Society of Japan*, **71**, 777–781.

[13] Ishihara, T., Kaneda, Y., Yokokawa, M., Itakura, K. and Uno, A., 2005, Energy spectrum in the near dissipation range of high resolution direct numerical simulation of turbulence. *Journal of Physics Society of Japan*, **74**, 1464–1471.

[14] Davidson, P.A., 2001, *An Introduction to Magnetohydrodynamics* (Cambridge: Cambridge University Press).

[15] Davidson, P.A., 2004, *Turbulence* (New York: Oxford University Press).

[16] Kaneda, Y., Ishihara, T., Yokokawa, M., Itakura, K. and Uno, A., 2003, Energy dissipation rate and energy spectrum in high resolution direct numerical simulations of turbulence in a periodic box. *Physics of Fluids*, **15**, L21–L24.

[17] Kaneda, Y., Ishihara, T., and Gotoh, K., 1999, Taylor expansions in powers of time of Lagrangian and Eulerian two-point two-time velocity correlations in turbulence. *Physics of Fluids*, **11**, 2154–2166.

[18] Ishihara, T., Yoshida, K. and Kaneda, Y., 2002, Anisotropic velocity correlation spectrum at small scales in a homogeneous turbulent shear flow. *Physical Review Letters*, **88**, 154501-1–154501-14.

[19] Yoshida, K., Ishihara, T. and Kaneda, Y., 2003, Anisotropic spectrum of homogeneous turbulent shear flow in a Lagrangian renormalized approximation. *Physics of Fluids*, **15**, 2385–2397.

[20] Yeung, P.K. and Pope, S.B., 1989, Lagrangian statistics from direct numerical simulations of isotropic turbulence. *Journal of Fluid Mechanics*, **207**, 531–586.

[21] Ishihara, T. and Kaneda, Y., 2002, Relative diffusion of a pair of fluid particles in the inertial subrange of turbulence. *Physics of Fluids*, **14**, 69–72.

[22] Sreenivasan, K.R., 1998, An update on the energy dissipation rate in isotropic turbulence. *Physics of Fluids*, **10**, 528–529.

[23] Ishihara, T., Yamazaki, Y. and Kaneda, Y., 2001, Statistics of small-scale structure of homogeneous. isotropic turbulence. In: T. Kambe, T. Nakano and T. Miyauchi (Eds) *IUTAM Symposium on Geometry and Statistics of Turbulence* (Dordrecht The Netherland: Kluwer Academic Publishers) pp. 133–138.

[24] Porter, D.H., Woodward, P.R. and Pouquet, A., 1998, Inertial range structures in decaying compressible turbulent flows. *Physics of Fluids*, **10**, 237–245.

[25] Ishihara, T., Kaneda, Y., Yokokawa, M., Itakura, K. and Uno, A., 2003, Spectra of energy dissipation, enstrophy and pressure by high-resolution direct numerical simulations of turbulence in a periodic box. *Journal of Physics Society of Japan*, **72**, 983–986.

[26] Martinez, D.O., Chen, S., Doolen, G.D., Kraichnan, R.H., Wang, L.-P., and Zhou, Y., 1997, Energy spectrum in the dissipation range of fluid turbulence. *Journal of Plasma Physics*, **57**, 195–201.

[27] Kaneda, Y. and Yoshida, K., 2004, Small-scale anisotropy in stably stratified turbulence. *New Journal of Physics*, **6**, 34.

[28] Moisy, F. and Jimenez, J., 2004, Geometry and clustering of intense structures in isotropic turbulence. *Journal of Fluid Mechanics*, **513**, 111–133.